Primary and Secondary Ferrocenylphosphine Complexes of Molybdenum(II) and Tungsten(II), $[MI_2(CO)_{3-n}(PH_2R)_{2+n}]$ [M = Mo, W; R = Fc, $FcCH_2$; Fc = $Fe(\eta^5\text{-}C_5H_5)(\eta^5\text{-}C_5H_4)$; n = 0, 1], $[MI_2(CO)_3\{PH(CH_2Fc)_2\}_2]$, and $[WI_2(CO)_3(NCMe)\{PH(CH_2Fc)_2\}]$: Preparation, Molecular Structure, Dynamic Behavior, Catalytic Properties, and Theoretical Calculations

René Sommer,[†] Peter Lönnecke,[†] Joachim Reinhold,[‡] Paul K. Baker,[§] and Evamarie Hey-Hawkins*,[†]

Institut für Anorganische Chemie der Universität Leipzig, Johannisallee 29, D-04103 Leipzig, Germany, Wilhelm-Ostwald-Institut für Physikalische und Theoretische Chemie der Universität Leipzig, Johannisallee 29, D-04103 Leipzig, Germany, and Department of Chemistry, University of Wales, Bangor, Gwynedd LL57 2UW, Wales, U.K.

Received March 16, 2005

Reaction of $[MI_2(CO)_3(NCMe)_2]$ [M = Mo, W] with 2 or 3 equiv of PH_2Fc or PH_2CH_2Fc [Fc = $Fe(\eta^5\text{-}C_5H_5)(\eta^5\text{-}C_5H_4)$] in CH_2Cl_2 or THF at various temperatures gave $[MI_2(CO)_3L_2]$ [M = Mo: L = PH_2Fc (**1a**), PH_2CH_2Fc (**2a**), $PH(CH_2Fc)_2$ (**5a**); M = W: L = PH_2Fc (**1b**), PH_2CH_2Fc (**2b**), $PH(CH_2Fc)_2$ (**5b**)] and $[MI_2(CO)_2L_3]$ [M = Mo: L = PH_2Fc (**3a**), PH_2CH_2Fc (**4a**); M = W: L = PH_2Fc (**3b**), PH_2CH_2Fc (**4b**)] in high yields. **2b** and **4a** were the first primary ferrocenylphosphine complexes of molybdenum(II) and tungsten(II) to be crystallographically characterized. Reaction of $[WI_2(CO)_3(NCMe)_2]$ with 1 equiv of $PH(CH_2Fc)_2$ in CH_2Cl_2 gave $[WI_2(CO)_3(NCMe)\{PH(CH_2Fc)_2\}]$ (**6**), the first structurally characterized tungsten(II) monophosphine complex with an acetonitrile ligand. All complexes show the structural motif of a capped octahedron. The formation of the bis-phosphine-substituted products is preferred when the reaction is carried out in a noncoordinating solvent at low temperatures, and with tungsten as the central atom, whereas coordinating solvents, higher temperatures, and molybdenum give rise to the formation of tris-phosphine-substituted products. VT ^{31}P NMR studies of **1**−**5** show fluxional behavior in solution. Density functional theory (DFT) calculations give insight into the reasons for the structural characteristics and the dynamic behavior of the complexes. Complexes **1**−**4** show only very low activity in the polymerization of norbornadiene.

1. Introduction

In previous years halo carbonyl complexes of molybdenum(II) and tungsten(II) complexes with a wide variety of ligands were described. An overview on their coordination chemistry is given in two reviews where, besides other complexes of the type $[MI_2(CO)_3L_2]$, a large number of complexes with group 15 donors were reported.[1,2] All of these complexes but one[3] bear *tertiary* phosphine ligands.[4−10] The coordination chemistry of these metals with primary and secondary phosphines was largely neglected, as most of these phosphines are highly air sensitive and therefore difficult to handle. However, as the steric and electronic properties of primary phosphines differ considerably from those of their tertiary counterparts, and these ligands have reactive P−H bonds, their corresponding transition metal complexes are of interest. In a recent communication[3] we reported the synthesis of the first primary ferrocenylphosphine complex of tungsten(II), $[WI_2$-

* To whom correspondence should be addressed. Fax: (+49)341-9739319. E-mail: hey@rz.uni-leipzig.de.
† Institut für Anorganische Chemie der Universität Leipzig.
‡ Wilhelm-Ostwald-Institut für Physikalische und Theoretische Chemie der Universität Leipzig.
§ University of Wales.

(1) Baker, P. K. *Adv. Organomet. Chem.* **1996**, *40*, 45−115, and references therein.
(2) Baker, P. K. *Chem. Soc. Rev.* **1998**, *27*, 125−131, and references therein.
(3) Sommer, R.; Lönnecke, P.; Baker, P. K.; Hey-Hawkins, E. *Inorg. Chem. Commun.* **2002**, 115−118.
(4) Baker, P. K.; Fraser, S. G. *Polyhedron* **1986**, *5*, 1381−1382.
(5) Baker, P. K.; Fraser, S. G. *Transition Met. Chem.* **1987**, *12*, 560−564.
(6) Baker, P. K.; Clark, A. I.; Meehan, M. M.; Parker, E. E.; Underhill, A. E.; Drew, M. G. B.; Durrant, M. C.; Richards, R. L. *Transition Met. Chem.* **1998**, *23*, 155−157.
(7) Al-Jahdali, M.; Baker, P. K.; Lavery, A. J.; Meehan, M. M.; Muldoon, D. J. *J. Mol. Catal. A* **2000**, *159*, 51−62.
(8) Baker, P. K.; Hursthouse, M. B.; Latif, L. A.; Abdul Malik, K. M. *J. Chem. Cryst.* **1998**, *28*, 639−643.
(9) Baker, P. K.; Coles, S. J.; Harrison, N. S.; Latif, L. A.; Meehan, M. M.; Hursthouse, M. B. *J. Organomet. Chem.* **1998**, *566*, 245−250.
(10) Drew, M. G. B.; Wilkins, J. D. *J. Chem. Soc., Dalton Trans.* **1977**, 194−197.

10.1021/om0501982 CCC: $30.25
Publication on Web 09/29/2005

Scheme 1. Reaction Scheme for the Stepwise Exchange of Acetonitrile and Carbonyl Ligands in $[MI_2(CO)_3(NCMe)_2]$ (M = Mo, W) by Primary or Sterically Demanding Secondary Phosphine Ligands

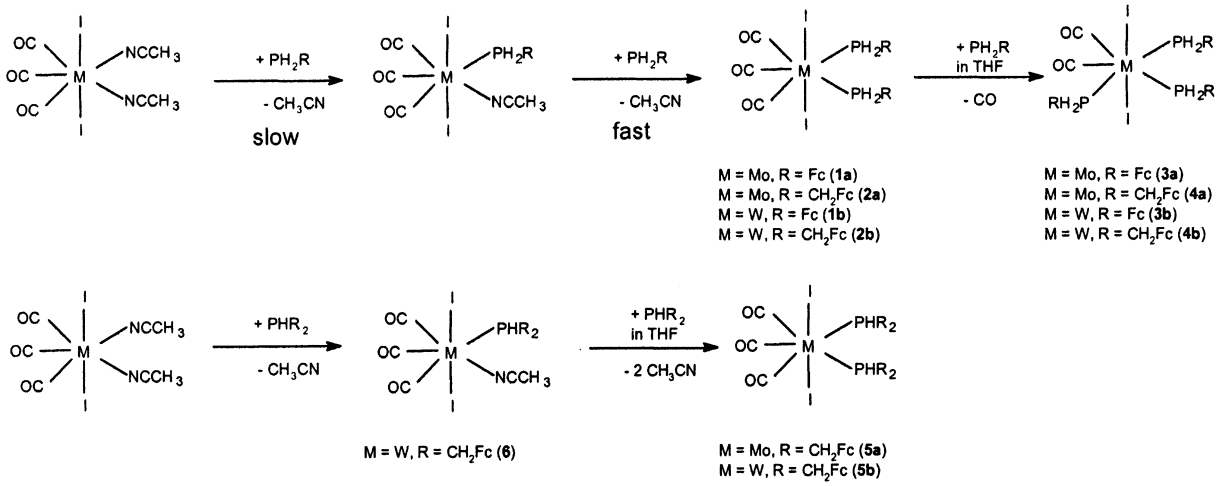

$(CO)_3(PH_2CH_2Fc)_2]$, which was obtained by treating $[WI_2(CO)_3(NCMe)_2]$ with 2 equiv of PH_2CH_2Fc [Fc = Fe-(η^5-C_5H_5)(η^5-C_5H_4)][11] in CH_2Cl_2. We now report the systematic investigation of the reactions between the seven-coordinate complexes $[MI_2(CO)_3(NCMe)_2]$ (M = Mo, W)[12] and primary (PH_2Fc,[13] PH_2CH_2Fc[11]) and secondary ferrocenylphosphines $[PH(CH_2Fc)_2]$,[14] including detailed experimental and theoretical studies of their molecular structures, their dynamic behavior in solution, and the reasons of the susceptibility of some of these complexes to ligand exchange beyond the expected limit. Since some Mo^{II} and W^{II} complexes are active single-component catalysts for the metathesis polymerization of norbornene and norbornadiene,[15−17] the catalytic properties of the corresponding complexes with primary phosphine ligands were studied.

2. Results and Discussion

2.1. Reactions of $[MI_2(CO)_3(NCMe)_2]$ (M = Mo, W) with Primary and Secondary Phosphines. Previous work on the coordination chemistry of phosphines in reactions with the seven-coordinate complexes $[MI_2(CO)_3(NCMe)_2]$ (M = Mo, W) showed that ligand exchange takes place in which the two labile acetonitrile ligands are subsequently replaced by phosphine ligands to give $[MI_2(CO)_3(PR_3)_2]$.[1,2,4−7] With 1 equiv of phosphine the 1:1 complex $[MI_2(CO)_3(NCMe)(PR_3)]$ is obtained, which dimerizes in most cases through iodo bridges and elimination of acetonitrile to give $[\{M(\mu\text{-}I)I(CO)_3(PR_3)\}_2]$.[2]

Correspondingly, the reaction of $[WI_2(CO)_3(NCMe)_2]$ with 2 equiv of PH_2Fc or PH_2CH_2Fc in CH_2Cl_2 gave $[WI_2(CO)_3L_2]$ [R = PH_2Fc (**1b**), PH_2CH_2Fc (**2b**)[3]]. However, when only 1 equiv of primary ferrocenylphosphine was employed, only **1b** and **2b** were formed, while the monosubstituted products $[WI_2(CO)_3(NCMe)L]$ or the iodo-bridged dimers $[\{W(\mu\text{-}I)I(CO)_3L\}_2]$ could not be observed by ^{31}P NMR spectroscopy. Apparently, the monophosphine-substituted complex reacts more rapidly with a phosphine than does the starting complex. A different behavior was observed for the corresponding molybdenum(II) complex $[MoI_2(CO)_3(NCMe)_2]$. The variable-temperature (VT) $^{31}P\{^1H\}$ NMR spectra of the products that were obtained with 1 or 2 equiv of PH_2Fc or PH_2CH_2Fc in CH_2Cl_2 showed that neither a 1:1 nor a 1:2 reaction had taken place; instead, the formation of the tris-phosphine-substituted products $[MoI_2(CO)_2L_3]$ [L = PH_2Fc (**3a**), PH_2CH_2Fc (**4a**)] was observed (Scheme 1).

We have therefore carried out more detailed studies to determine the required reaction conditions (solvent, temperature) for the preferred or even clean formation of either the disubstituted complexes $[MI_2(CO)_3L_2]$ [M = Mo: L = PH_2Fc (**1a**), PH_2CH_2Fc (**2a**); M = W: L = PH_2Fc (**1b**), PH_2CH_2Fc (**2b**)] or the trisubstituted complexes $[MI_2(CO)_2L_3]$ [M = Mo: L = PH_2Fc (**3a**), PH_2CH_2Fc (**4a**); M = W: L = PH_2Fc (**3b**), PH_2CH_2Fc (**4b**)] in high yields. Since the starting materials and the products are soluble in the coordinating solvent THF as well as in noncoordinating chlorinated solvents such as CH_2Cl_2, differences in the reaction pathways in these two solvents were studied. At room temperature, $[MoI_2(CO)_3(NCMe)_2]$ gave the tris-phosphine-substituted complexes **3a** and **4a** much more readily than $[WI_2(CO)_3(NCMe)_2]$ regardless of the solvent (although a cleaner reaction was observed in THF, while 5 to 10% of $[MoI_2(CO)_3(PH_2R)_2]$ (**1a**, **2a**) was formed in CH_2Cl_2; reaction time > 10 min). Accordingly, at −30 °C and short reaction times (5−10 min) product mixtures were obtained that contain up to 85% $[MoI_2(CO)_3L_2]$ [L = PH_2Fc (**1a**), PH_2CH_2Fc (**2a**)] besides the trisubstituted complexes **3a** and **4a**. However, while short reaction times reduce the amount of tris-phosphine-substituted complex a lower overall yield is also observed. Attempts to separate the di- and trisubstituted products by fractional crystallization failed.

In contrast, the tris-phosphine-substituted tungsten complexes **3b** and **4b** were not formed in CH_2Cl_2 or if

(11) (a) Goodwin, N. J.; Henderson, W.; Nicholson, B. K. *Chem. Commun*. **1997**, 31−32. (b) Goodwin, N. J.; Henderson, W.; Nicholson, B. K.; Fawcett, J.; Russell, D. R. *J. Chem. Soc., Dalton Trans*. **1999**, 1785−1793.
(12) Baker, P. K.; Fraser, S. G.; Keys, E. M. *J. Organomet. Chem.* **1986**, *309*, 319−321.
(13) Spang, C.; Edelmann, F. T.; Noltemeyer, M.; Roesky, H. W. *Chem. Ber.* **1989**, *122*, 1247−1254.
(14) Sommer, R.; Lönnecke, P.; Hey-Hawkins, E. *Dalton Trans.* Manuscript in preparation.
(15) Bencze, L.; Kraut-Vass, A. *J. Organomet. Chem.* **1984**, *270*, 211−220.
(16) Bencze, L.; Kraut-Vass, A. *J. Mol. Catal.* **1985**, *28*, 369−380.
(17) Szymańska-Buzar, T.; Głowiak, T.; Czeluśniak, I. *J. Organomet. Chem.* **2001**, *640*, 72−78.

Table 1. Crystal Data and Structure Refinement for 4a and 6

	4a	6
empirical formula	$C_{35}H_{39}Fe_3I_2MoO_2P_3$	$C_{27}H_{26}Fe_2I_2NO_3PW \cdot CH_2Cl_2$
fw	1101.86	1077.73
temperature	216(2) K	223(2) K
wavelength	71.073 pm	71.073 pm
cryst syst	triclinic	monoclinic
space group	$P\bar{1}$	$P2_1/n$
unit cell dimens	a = 1249.13(14) pm	a = 1272.70(13) pm
	b = 1320.25(15) pm	b = 1505.11(16) pm
	c = 1343.94(15) pm	c = 1754.99(19) pm
	α = 65.756(2)°	α = 90°
	β = 67.822(2)°	β = 97.113(2)°
	γ = 77.505(2)°	γ = 90°
volume	1.8664(4) nm^3	3.3359(6) nm^3
Z	2	4
density (calcd)	1.961 g/cm^3	2.146 g/cm^3
absorp coeff	3.285 mm^{-1}	6.387 mm^{-1}
F(000)	1072	2032
cryst size	0.25 × 0.20 × 0.08 mm^3	0.20 × 0.10 × 0.10 mm^3
θ range for data collection	1.70−28.90°	1.79−26.37°
index ranges	$-14 \le h \le 16$; $-17 \le k \le 15$; $-17 \le l \le 17$	$-12 \le h \le 15$; $-16 \le k \le 18$; $-19 \le l \le 21$
no. of reflns collected	12 292	19 653
no. of indep reflns	8532 [R(int) = 0.0285]	6810 [R(int) = 0.0580]
completeness to θ_{max}	to θ = 28.90°: 86.8%	to θ = 26.37°: 99.8%
absorp corr	SADABS[37]	SADABS[37]
no. of restraints/params	0/431	0/366
goodness-of-fit on F^2	1.026	1.005
final R indices [$I>2\sigma(I)$]	R1 = 0.0363, wR2 = 0.0822	R1 = 0.0400, wR2 = 0.0910
R indices (all data)	R1 = 0.0604, wR2 = 0.1043	R1 = 0.0798, wR2 = 0.1129
largest diff peak and hole	0.725 and −1.007 e Å^{-3}	0.933 and −1.785 e Å^{-3}

the reaction time in THF was too short. In these cases solely the formation of the bis-phosphine-substituted products **1b** and **2b** was observed. The influence of the reaction time on the reaction of $[WI_2(CO)_3(NCMe)_2]$ with 3 equiv of PH_2CH_2Fc in THF at room temperature was studied by ^{31}P NMR spectroscopy. The observed increase in the yield of $[WI_2(CO)_2(PH_2CH_2Fc)_3]$ (**4b**) from 30% [besides 70% $[WI_2(CO)_3(PH_2CH_2Fc)_2]$ (**2b**)] after 5 min to nearly 100% after 2 h shows that the tris-phosphine-substituted product is formed via the bis-phosphine complex.

The reaction of $[MI_2(CO)_3(NCMe)_2]$ (M = Mo, W) with more than two monodentate phosphine ligands to yield a tris-phosphine-substituted product was not observed so far. However, Umland and Vahrenkamp[18] reported the synthesis of the only other known tris-phosphine-substituted complexes $[MX_2(CO)_2(PMe_3)_3]$ (M = Mo, W; X = Cl, Br, I), which were obtained from $[\{Mo(\mu\text{-}X)X(CO)_4\}_2]$ or $[WX_2(CO)_4(PMe_3)]$ and PMe_3. As far as monodentate tertiary phosphine ligands are concerned, this reaction occurs exclusively with PMe_3[18] and PMe_2Ph[10,19] (for similar reactions with chelating ligands, e.g., $PPh_2CH{=}CHPPh_2$, see ref 20). We thus concluded that sterically less demanding phosphine ligands, such as the primary ferrocenylphosphines PH_2Fc and PH_2CH_2Fc, are necessary to form tris-phosphine-substituted complexes.

We could demonstrate the uniqueness of primary ferrocenylphosphine ligands in their ability to form tris-phosphine-substituted complexes from $[MI_2(CO)_3(NCMe)_2]$ (M = Mo, W) by replacing PH_2CH_2Fc by the secondary phosphine $PH(CH_2Fc)_2$.[14] When reaction conditions were applied that in the case of primary ferrocenylphosphines led to the formation of tris-phosphine-substituted complexes (THF, room temperature, reaction times of several hours), only the bis-phosphine complexes $[MI_2(CO)_3L_2]$ [M = Mo, L = $PH(CH_2Fc)_2$ (**5a**); M = W, L = $PH(CH_2Fc)_2$ (**5b**)] were formed. Moreover, when $[WI_2(CO)_3(NCMe)_2]$ was treated with $PH(CH_2Fc)_2$ in CH_2Cl_2 at 20 °C, that is, conditions under which primary ferrocenylphosphines resulted in the formation of bis-phosphine complexes, the unprecedented formation of a stable, crystalline, monomeric monophosphine complex that still contains one acetonitrile ligand $[WI_2(CO)_3(NCMe)\{PH(CH_2Fc)_2\}]$ (**6**) took place (Scheme 1).

2.2. Nomenclature for Capped Octahedral Structures.[21] To date, IUPAC has not provided any stereodescriptive nomenclature beyond the recommended polyhedral symbols (e.g., *OCF*-7) for complexes with the basic structural motif of an octahedron and a coordination number higher than 6. However, in a paper by Sloan et al., the configuration index for such structures is produced by listing the CIP priority numbers for all ligands in a defined sequence,[22] and we propose to employ this approach also for the capped octahedral complexes described here.

2.3. Crystal Structures. Single crystals suitable for X-ray crystallography were obtained from a concentrated solution of **2b** in THF at −20 °C or **4a** in $CHCl_3$ at −30 °C (after 2 days). Single crystals of **6** were obtained from CH_2Cl_2 at −20 °C.

The structures were solved by direct methods[23] and refined by using a full-matrix least-squares algorithm.[24] The crystal structure and refinement data for compounds **4a** and **6** are given in Table 1; the respective data for **2b** were reported earlier.[3]

(18) Umland, P.; Vahrenkamp, H. *Chem. Ber.* **1982**, *115*, 3565−3579.
(19) Mawby, A.; Pringle, G. E. *J. Inorg. Nucl. Chem.* **1972**, *34*, 517−524.
(20) Baker, P. K.; Drew, M. G. B.; Johans, A. W.; Latif, L. A. *J. Organomet. Chem.* **2000**, *602*, 115−124.
(21) We are presently preparing the full proposal "Extension of IUPAC Rules for Stereo Descriptors to Coordination Numbers 7-12" for IUPAC. Hey-Hawkins, E.; Sommer, R.; Leigh, J.; Hartshorn, R. M. In preparation.
(22) Brown, M. F.; Cook, B. R.; Sloan, T. E. *Inorg. Chem.* **1978**, *17*, 1563−1568.

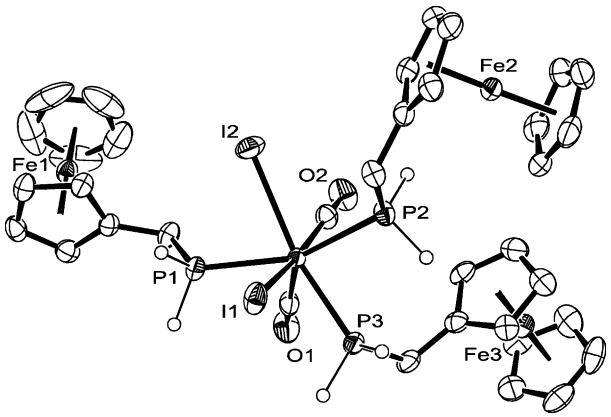

Figure 1. ORTEP plot of $[MoI_2(CO)_2(PH_2CH_2Fc)_3]$ (**4a**) (hydrogen atoms other than PH are omitted for clarity; ellipsoids are shown with 50% probability).[37] Selected bond lengths (pm) and bond angles (deg): Mo(1)−I(1) 288.3(1), Mo(1)−I(2) 286.4(1), Mo(1)−C(34) 193.5(5), Mo(1)−C(35) 195.6(5), Mo(1)−P(1) 246.7(1), Mo(1)−P(2) 256.1(1), Mo(1)−P(3) 245.3(1), C(34)−O(1) 116.6(6), C(35)−O(2) 115.5(6), C(34)−Mo(1)−C(35) 73.4(2), C(34)−Mo(1)−P(1) 73.7(2), C(34)−Mo(1)−P(2) 132.8(2), C(34)−Mo(1)−P(3) 73.7(2), C(35)−Mo(1)−P(1) 107.7(2), C(35)−Mo(1)−P(2) 80.8(2), C(35)−Mo(1)−P(3) 110.5(2), P(1)−Mo(1)−P(2) 153.1(1), P(1)−Mo(1)−P(3) 118.8(1), P(2)−Mo(1)−P(3) 79.5(1), P(1)−Mo(1)−I(2) 75.2(1), P(2)−Mo(1)−I(2) 81.8(1), P(3)−Mo(1)−I(2) 157.4(1), C(34)−Mo(1)−I(2) 128.8(2), C(35)−Mo(1)−I(2) 78.7(2), C(34)−Mo(1)−I(1) 120.8(2), C(35)−Mo(1)−I(1) 165.7(2), P(1)−Mo(1)−I(1) 78.11(3), P(2)−Mo(1)−I(1) 88.43(3), P(3)−Mo(1)−I(1) 76.34(3), I(1)−Mo(1)−I(2) 90.59(2).

Crystals obtained for the other complexes were not suitable for X-ray crystallography. The parts of this paper concerning fluxional behavior and the theoretical calculations are therefore based on the assumption that the structural motifs of all bis-phosphine complexes $[MI_2(CO)_3(PH_2R)_2]$ and all tris-phosphine complexes $[MI_2(CO)_2(PH_2R)_3]$ (M = Mo, W) are similar.

General Features. All three complexes **2b**,[3] **4a** (Figure 1), and **6** (Figure 2) have a distorted capped octahedral geometry in which a CO ligand occupies the capping position of an octahedral face, which includes the other one or two CO ligands, respectively. The smallest distortion occurs for the iodo ligands (the I−M−I bond angles in **2b**, **4a**, and **6** are close to 90°), the P−M−P bond angle in bis-phosphine-substituted complexes is smaller than 180°, and complexes with primary phosphine ligands have smaller P−M−P bond angles than complexes with tertiary phosphine ligands (e.g., **2b**[3] 150.5(1)°, $[WI_2(CO)_3(PEt_3)_2]$[6] 164.72(9)°, $[MoCl_2(CO)_3(PEt_3)_2]$,[10] 161.5(3)°), which also agrees with the theoretical calculations (Table 2).

$[WI_2(CO)_3(PH_2CH_2Fc)_2]$ (2b). Compound **2b** shows a capped octahedral structure. The complex exhibits a major deviation from the ideal capped octahedral structure, but quite well reflects the angle proportions of the "conventional capped octahedron" as proposed by Drew.[25,26] The structure was already described in our preliminary communication.[3] In **2b**, the carbonyl group C(23)−O(1) occupies the capping position of a face of one phosphine and two CO ligands. The atoms I(1), I(2), C(24), and C(25) form the equatorial plane, with the two phosphine ligands occupying the axial positions.

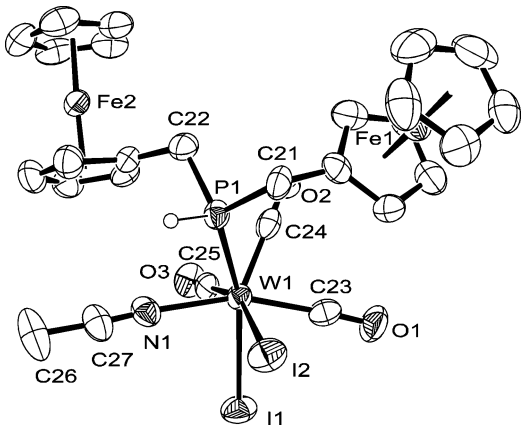

Figure 2. ORTEP plot of $[WI_2(CO)_3(NCMe)\{PH(CH_2Fc)_2\}]$ (**6**) (hydrogen atoms other than PH are omitted for clarity; ellipsoids are shown with 50% probability).[37] Selected bond lengths (pm) and bond angles (deg): W(1)−C(23) 200.8(9), W(1)−C(24) 197.3(9), W(1)−C(25) 200.5(9), W(1)−N(1) 218.4(7), W(1)−P(1) 250.3(2), W(1)−I(2) 285.3(1), W(1)−I(1) 287.3(1), C(23)−O(1) 115.4(10), C(24)−O(2)113.8(9), C(25)−O(3) 114.4(9), C(23)−W(1)−C(24) 76.7(3), C(23)−W(1)−C(25) 106.8(3), C(24)−W(1)−C(25) 71.5(3), C(23)−W(1)−N(1) 160.1(3), C(24)−W(1)−N(1) 123.1(3), C(25)−W(1)−N(1) 81.6(3), C(23)−W(1)−P(1) 113.6(2), C(24)−W(1)−P(1) 72.6(2), C(25)−W(1)−P(1) 116.4(2), N(1)−W(1)−P(1) 76.5(2), C(23)−W(1)−I(1) 78.0(2), C(24)−W(1)−I(1) 129.5(2), C(25)−W(1)−I(1) 75.1(2), N(1)−W(1)−I(1) 87.2(2), P(1)−W(1)−I(1) 157.8(1), C(23)−W(1)−I(2) 80.0(2), C(24)−W(1)−I(2) 129.0(2), C(25)−W(1)−I(2) 159.4(2), N(1)−W(1)−I(2) 86.3(2), P(1)−W(1)−I(2) 76.4(1), I(1)−W(1)−I(2) 87.78(2).

Table 2. Selected Structural Parameters (pm and deg) Resulting from the Calculations for the Bis-phosphine Model Complexes $[MI_2(CO)_3(PR_3)_2]$ (M = Mo, W; R = H, Me)

	M = Mo		M = W	
	R = H	R = Me	R = H	R = Me
$M-C_{equ}$	202.9	201.4	201.6	200.4
$C_{equ}-O_{equ}$	115.1	115.4	115.4	115.7
$M-C_{cap}$	198.9	197.0	199.0	197.3
$C_{cap}-O_{cap}$	115.8	116.3	116.0	116.6
M−I	297.0	300.4	296.3	299.0
$M-P_{ax}$	258.9	267.1	256.6	265.3
$M-P_{ax/cap}$[a]	249.9	259.5	250.2	259.0
I−M−I	91.4	95.2	89.2	92.6
$P_{ax/cap}-M-P_{ax}$	148.7	155.6	150.9	157.0
$P_{ax/cap}-M-C_{cap}$	75.3	72.2	75.9	72.8
$P_{ax}-M-C_{equ}$	80.2	79.1	79.7	79.1
$C_{equ}-M-C_{equ}$	111.7	110.6	112.5	111.2
$C_{cap}-M-C_{equ}$	75.6	74.3	74.8	73.5

[a] $P_{ax/cap}$ denotes the P atom in the neighborhood of the capping CO ligand.

$[MoI_2(CO)_2(PH_2CH_2Fc)_3]$ (4a). Compound **4a** (Figure 1) is the first structurally characterized complex of the type $[MI_2(CO)_2L_3]$ (M = Mo, W; L = phosphine). The ferrocenylphosphine ligands are in a meridional conformation and thus avoid each other's steric influence optimally. C(34) occupies the capping position over a face of one CO and two phosphine ligands. The C(34)−Mo−C(35) [or P(1), P(3)] bond angles are small [73.4-

(23) Sheldrick, G. M. *SHELXS-97*, Program for Crystal Structure Solution; Universität Göttingen, 1997.
(24) *SHELXTL PLUS*, *XS*: Program for Crystal Structure Solution, *XL*: Program for Crystal Structure Determination, *XP*: Interactive Molecular Graphics; Siemens Analytic X-ray Instruments Inc., 1990.
(25) Drew, M. G. B.; Wolters, A. P. *Chem. Commun.* **1972**, 457−458.
(26) Drew, M. G. B. *Progr. Inorg. Chem.* **1977**, *23*, 67−210.

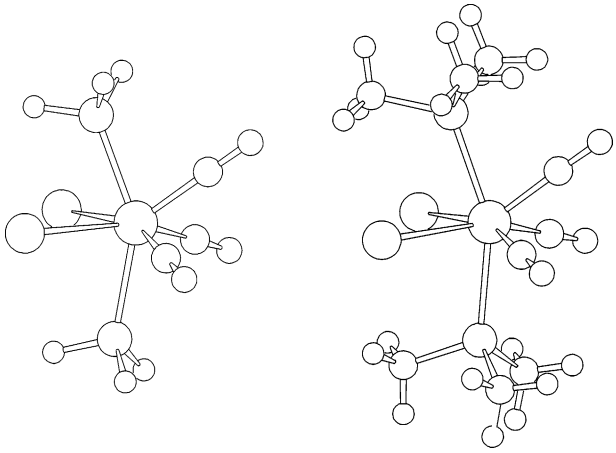

Figure 3. SCHAKAL plot of the optimized structures of $[MI_2(CO)_3(PR_3)_2]$ (left: R = H, right: R = Me).

(2)−73.7(2)°]. The two iodo ligands occupy two of the remaining three octahedral sites with a *cis* arrangement [I(1) *trans* to C(35), I(2) *trans* to P(3)].

As in **2b**, the phosphine ligands show major deviations from their ideal octahedral positions with P−Mo−P bond angles of 153.1°, 118.8°, and 79.5°, as opposed to the ideal values of 180°, 90°, and 90°, due to the distortion caused by the capping CO group. However, the angles observed in **4a** are close to those in the "conventional capped octahedron".[25,26]

$[WI_2(CO)_3(NCMe)\{PH(CH_2Fc)_2\}]$ (6). Compound **6** (Figure 2) is the first structurally characterized complex of seven-coordinate tungsten(II) containing one acetonitrile ligand together with one phosphine ligand. Complexes of the type $[MI_2(CO)_2(NCMe)L]$ (M = Mo, W) usually tend to dimerize with elimination of acetonitrile and formation of iodo bridges,[2] whereas in **6** dimerization appears to be inhibited by the steric bulk of the bis(ferrocenylmethyl)phosphine ligand. In **6**, the carbonyl group C(24)−O(2) caps the face that includes the phosphine and the other two CO ligands. The acetonitrile ligand lies in the equatorial plane, *trans* to the carbonyl group C(23)−O(1). One iodo ligand is *trans* to the phosphine, and the other (I(2)) *trans* to the carbonyl group C(25)−O(3).

To provide a systematic description of the structural peculiarities of the considered class of compounds, geometry optimizations (see Experimental Section, 3.11) were carried out for a variety of suitable model complexes. Instead of the rather large ferrocenyl-substituted primary phosphines, for which the formation of tris-phosphine-substituted complexes was observed, the model ligand PH_3 was used. As a representative of the secondary and tertiary phosphines, for which this tendency is not observed, the PMe_3 ligand was chosen (although PMe_3 is the only known tertiary phosphine ligand that has the ability to form tris-phosphine-substituted seven-coordinate Mo^{II} and W^{II} complexes, but the reaction conditions described by Umland and Vahrenkamp[18] show that this tendency is presumably far less pronounced than for primary phosphines).

Four bis-phosphine complexes $[MI_2(CO)_3(PR_3)_2]$ (M = Mo, W; R = H, Me) were considered. Complete geometry optimizations were performed adopting a capped octahedral complex structure and preserving C_s symmetry. The stationary points were characterized by frequency analyses. The PH_3 complexes are minima on the potential surface, whereas for the PMe_3 derivatives one imaginary frequency (14i and 28i for the Mo and W system, respectively) occurs, which refers to a slight turning of the axial PMe_3 group around the local 3-fold axis but not to a distortion of the capped octahedral coordination polyhedron. In Figure 3, the resulting overall structures are displayed. Selected structural parameters are presented in Table 2.

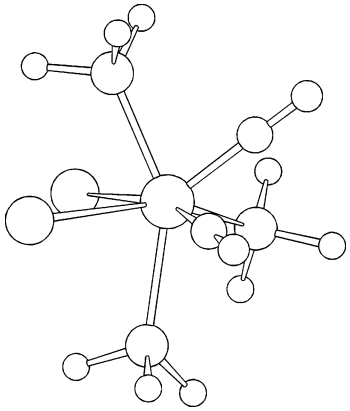

Figure 4. SCHAKAL plot of the optimized structure of $[MI_2(CO)_2(PH_3)_3]$.

Table 3. Selected Structural Parameters (pm and deg) Resulting from the Calculations for the Tris-phosphine Model Complexes $[MI_2(CO)_2(PH_3)_3]$ (M = Mo, W)

	M = Mo	M = W
$M-C_{equ}$	200.1	199.0
$C_{equ}-O_{equ}$	115.6	115.9
$M-C_{cap}$	197.2	197.1
$C_{cap}-O_{cap}$	116.4	116.8
M−I (*trans* CO)	299.7	299.2
M−I (*trans* PH_3)	296.4	295.3
$M-P_{ax}$	258.8	255.8
$M-P_{ax/cap}$[a]	248.6	248.7
$M-P_{equ}$	250.1	249.2
I−M−I	91.0	88.6
$P_{ax/cap}-M-P_{ax}$	148.8	151.5
$P_{ax/cap}-M-C_{cap}$	75.7	76.4
$C_{equ}-M-P_{equ}$	113.0	114.8
$C_{cap}-M-P_{equ}$	73.5	73.1
$C_{cap}-M-P_{equ}$	75.7	74.8

[a] $P_{ax/cap}$ denotes the P atom in the neighborhood of the capping CO ligand.

Regarding the tris-phosphine-substituted complexes, complete geometry optimizations (C_1 symmetry) of the model systems $[MI_2(CO)_2(PH_3)_3]$ (M = Mo, W) yield a minimum structure with the third phosphine ligand occupying an equatorial position (Figure 4), in agreement with the experimental structure of complex **4a** (Figure 1). In Table 3, selected structural parameters are given.

For both types of complexes, the calculations reproduce well the essential structural peculiarities found in the experiments, such as the bond angles and, especially, the M−C and C−O bond lengths (cf. Figure 1 and ref 3). From the available experimental data and from Tables 2 and 3, the following structural features can be derived: The M−C distances are generally larger for (a) molybdenum versus tungsten, (b) PH_3 versus PMe_3, and (c) the equatorial versus the capping position. The C−O distances show exactly the opposite behavior.

Table 4. Wavenumbers (cm^{-1}) of the CO and PH Stretching Vibrations of Complexes 1−6 (in KBr)

complex	ν(CO)	ν(PH)
$[MoI_2(CO)_3(PH_2Fc)_2]$ (**1a**)[a]	2029s, 2003m, *1962s*, 1934sh	2310w, 2278m
$[WI_2(CO)_3(PH_2Fc)_2]$ (**1b**)	2022s, 1945s, 1917s	2344m
$[MoI_2(CO)_3(PH_2CH_2Fc)_2]$ (**2a**)[a]	2033s, 2001m, 1964s, *1847m*	2345w, 2278w
$[WI_2(CO)_3(PH_2CH_2Fc)_2]$ (**2b**)	2018s, 1951s, 1917s	2356m
$[MoI_2(CO)_2(PH_2Fc)_3]$ (**3a**)	1955s, 1874s	2333m
$[WI_2(CO)_2(PH_2Fc)_3]$ (**3b**)	1945s, 1857s	2362w, 2320m, 2298w
$[MoI_2(CO)_2(PH_2CH_2Fc)_3]$ (**4a**)	1947s, 1848s	2344m, 2332m
$[WI_2(CO)_2(PH_2CH_2Fc)_3]$ (**4b**)	1938s, 1835s	2330m
$[MoI_2(CO)_3\{PH(CH_2Fc)_2\}_2]$ (**5a**)	2024s, 1945s, 1861s	2336m
$[WI_2(CO)_3\{PH(CH_2Fc)_2\}_2]$ (**5b**)	2019s, 1942s, 1920s	2351m
$[WI_2(CO)_3(NCMe)\{PH(CH_2Fc)_2\}]$ (**6**)	2021s, 2000s, 1939s	2315w, 2287w[b]

[a] Compound could not be obtained in pure form, so that a superposition with the absorption bands of the tris-phosphine-substituted complex **3a** or **4a** may occur. IR bands that also appear in the spectrum of **3a** or **4a** are in italics. [b] One absorption is due to ν(CN).

Table 5. Wavenumbers of the CO Stretching Vibrations (cm^{-1}) Resulting from the Calculations for the Model Complexes $[MI_2(CO)_3(PR_3)_2]$ (M = Mo, W; R = H, Me) and $[MI_2(CO)_2(PH_3)_3]$ (M = Mo, W)

	M = Mo		M = W	
	R = H	R = Me	R = H	R = Me
Bis-phosphine Complexes				
a′ $C_{cap}-O_{cap}$	2043	2009	2031	1997
a″ $C_{equ}-O_{equ}$ asym	2075	2048	2060	2034
a′ $C_{equ}-O_{equ}$ sym	2122	2098	2115	2092
Tris-phosphine Complexes				
$C_{cap}-O_{cap}$	2004		1989	
$C_{equ}-O_{equ}$	2073		2061	

Table 6. Mulliken Charges Resulting from the Calculations for the Bis-phosphine Model Complexes $[MI_2(CO)_3(PR_3)_2]$ (M = Mo, W; R = H, Me)

	M = Mo		M = W	
	R = H	R = Me	R = H	R = Me
M	−0.44	−0.40	−0.55	−0.51
$(CO)_{equ}$	0.03	0.00	0.00	−0.04
$(CO)_{cap}$	−0.06	−0.12	−0.26	−0.29
I	−0.17	−0.27	−0.13	−0.22
$(PR_3)_{ax}$	0.40	0.55	0.46	0.61
$(PR_3)_{ax/cap}$[a]	0.38	0.51	0.45	0.57

[a] $P_{ax/cap}$ denotes the P atom in the neighborhood of the capping CO ligand.

These findings can be related to the M−CO bond strengths (vide infra).

2.4. IR Spectroscopic Investigations. The M−C(O) vibrations of **1**−**6** were not easily identified due to their low intensity and their location in the fingerprint region of the IR spectrum. Commonly, the strength of the CO bond is related to the strength of the metal−carbonyl bond. Thus, it should be possible to gain insight into the strength of the metal−carbonyl bonds by examining the wavenumbers of the strong IR bands of the CO groups (Table 4).

Substitution of one of the three CO ligands by a third phosphine ligand shifts the CO absorption bands to lower wavenumbers, which indicate stronger M−C bonds in the tris-phosphine complexes. Table 5 presents the calculated wavenumbers of the C−O stretching vibrations of the model complexes. The comparison with the experimental values for the real complexes (Table 4) and with the values published for $[WI_2(CO)_3(PMe_3)_2]$ (1908, 1945, and 2017 cm^{-1})[18] shows that the calculated values are generally somewhat too large. The differences between the individual wavenumbers, however, appear to be reliable.

For the bis-phosphine model complexes, the frequency analyses attribute, in each case, the lowest wavenumber definitely to the stretching vibration of the unique capping carbonyl ligand. This is in contradiction to former assignments,[3,5] which associated this vibration with the highest wavenumber on the basis of the assumption that the capping carbonyl may be less tightly bound to the metal center. The analyses show that the vibration with the highest wavenumber belongs to the symmetric stretching vibration of the two equatorial carbonyl groups. The intermediate wavenumber is assigned to the asymmetric vibration of these two groups. For the tris-phosphine complexes, the frequency analyses attribute, correspondingly, the lower value to the capping carbonyl group and the higher value to the equatorial one.

In agreement with the experimental results, the calculated values show that larger wavenumbers of the stretching vibrations correspond to shorter C−O bond lengths. Thus, the strongest C−O bond and, correspondingly, the weakest M−C bond is observed for the equatorial CO ligands in $[MoI_2(CO)_3(PH_3)_2]$. Replacement of molybdenum by tungsten or of PH_3 by the tertiary phosphine PMe_3 weakens the C−O bonds and strengthens the M−carbonyl bonds. Generally, the capping CO ligand is more strongly bound to the metal center than the equatorial ones. In agreement with the usual bonding situation, the strict inverse relationship between the M−CO and the C−O bonds in terms of both bond lengths and strengths indicates that the metal−carbonyl bonds are determined by their π-acceptor character.

To obtain insight into the influence of the specific metal center and the phosphine ligands on the metal−carbonyl bonds, the Mulliken charges of the individual atoms and ligands in the bis-phosphine model systems were examined (Table 6).

The values clearly indicate that PMe_3 is, as expected, a stronger σ donor than PH_3 and that the phosphine donor capability is more efficient in the tungsten complex. The smallest back-donation appears for the equatorial metal−carbonyl bonds in $[MoI_2(CO)_3(PH_3)_2]$, indicating these bonds to be the weakest ones in accordance with the resulting bond lengths and stretching frequencies.

The role of the different phosphine ligands is relatively easy to explain. Independent of the metal, the increased donor ability of the trimethylphosphine ligands increases the π donation of the electrons from the metal

Table 7. ^{31}P NMR Chemical Shifts and Coupling Constants $^1J_{P,H}$ of the Free Phosphines and Complexes 1−6 at 27 °C in $CDCl_3$

	δ (ppm)	$^1J_{P,H}$ (Hz)	Δ ($\delta_{complex}-\delta_{ligand}$) (ppm)	Δ ($^1J_{P,H\ (complex)} - {}^1J_{P,H\ (ligand)}$) (Hz)
		Free Phosphines		
PH_2Fc	−144.5	199		
PH_2CH_2Fc	−129.1	194		
$PH(CH_2Fc)_2$	−53.4	196		
		Complexes		
$[MoI_2(CO)_3(PH_2Fc)_2]$ (**1a**)	−56.8	398[a]	87.7	199
$[WI_2(CO)_3(PH_2Fc)_2]$ (**1b**)	−75.0	402[a]	69.5	203
$[MoI_2(CO)_3(PH_2CH_2Fc)_2]$ (**2a**)	−52.4	378[a]	76.7	184
$[WI_2(CO)_3(PH_2CH_2Fc)_2]$ (**2b**)	−70.3	385[b]	58.8	191
$[MoI_2(CO)_2(PH_2Fc)_3]$ (**3a**)	−40.4	384	104.1	185
$[WI_2(CO)_2(PH_2Fc)_3]$ (**3b**)	−60.9	385[b]	83.6	186
$[MoI_2(CO)_2(PH_2CH_2Fc)_3]$ (**4a**)	−34.5	363	94.6	169
$[WI_2(CO)_2(PH_2CH_2Fc)_3]$ (**4b**)	−55.2	369	73.9	175
$[MoI_2(CO)_3\{PH(CH_2Fc)_2\}_2]$ (**5a**)	+6	389[b]	59.4	193
$[WI_2(CO)_3\{PH(CH_2Fc)_2\}_2]$ (**5b**)	ca. −15[d]	401[c]	ca. 38	205
$[WI_2(CO)_3(NCMe)\{PH(CH_2Fc)_2\}]$ (**6**)	+7.6	391	61.0	195

[a] Higher order ^{31}P NMR spectrum. $^1J_{P,H}$ was taken from the ^{1}H NMR spectrum. [b] ^{31}P NMR signal too broad; $^1J_{P,H}$ was taken from the ^{1}H NMR spectrum. [c] Average $^1J_{P,H}$ at −50 °C is given. [d] At 40 °C; no signal was observed at rt (^{31}P NMR signal shows coalescence at 30 °C).

to the carbonyl ligands, thus strengthening the M−CO bonds. The role of the different metal centers also corresponds to what was expected. From the calculations, it results that, independent of the specific phosphine ligand, the carbonyl groups accept more electron density from a tungsten than from a molybdenum center, leading to stronger M−CO bonds for tungsten. This corresponds to the experience that CO is generally more strongly bound to tungsten than to molybdenum. In fact, it has been calculated that the first bond dissociation energy of the M−CO bond in mononuclear metal carbonyl complexes is higher for third-row transition metals than for their second-row counterparts.[27] Corresponding results were obtained for the respective bond lengths.[28,29] We have carried out comparative optimizations for $Mo(CO)_6$ and $W(CO)_6$, which have yielded the following bond distances: Mo−C = 207.9 pm, C−O = 114.9 pm and W−C = 206.8 pm, C−O = 115.1 pm, respectively.

The P−H stretching vibrations appear in the same region for all complexes, with the strongest bands all above 2300 cm^{-1}. As is observed for other ferrocenylphosphine complexes,[30] the P−H stretching vibrations were shifted to higher wavenumbers compared to the free phosphines (PH_2Fc 2225 cm^{-1};[13] PH_2CH_2Fc 2285 cm^{-1};[11b] $PH(CH_2Fc)_2$ 2285 cm^{-1} [14]).

2.5. NMR Spectroscopic Investigations. On coordination of the phosphines PH_2Fc, PH_2CH_2Fc, and $PH(CH_2Fc)_2$ to Mo^{II} or W^{II}, a downfield shift of the ^{31}P NMR signal of 59 to 104 ppm for molybdenum and 38 to 83 ppm for tungsten can be observed, combined with an increase in the $^1J_{P,H}$ coupling constant from ca. 200 Hz in the free phosphines[11,14] to ca. 360−405 Hz in the complexes (always slightly higher in W compared to Mo complexes, Table 7). The downfield shift of the ^{31}P NMR signal is generally larger by ca. 15 ppm for the tris-phosphine-substituted complexes in comparison with their bis-phosphine-substituted analogues, whereas the coupling constant $^1J_{P,H}$ is smaller. On the other hand, the mono-phosphine complex **6** shows a downfield shift that is ca. 20 ppm larger than that of complex **5b** (accompanied by a smaller $^1J_{P,H}$ coupling constant, Table 7) so that the changes in chemical shift and coupling constant of the ferrocenylphosphines on complex formation cannot be correlated directly with the number of phosphine or CO ligands in the molecule.

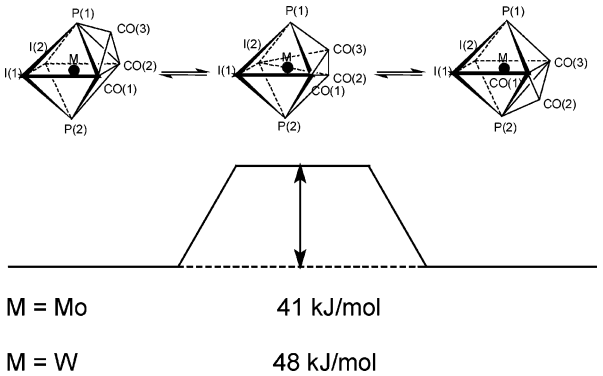

Figure 5. Energy profile for the pseudorotation of the $(CO)_3$ moiety in the model complexes $[MI_2(CO)_3(PH_3)_2]$ (M = Mo, W).

In the proton-decoupled ^{31}P NMR spectra of all complexes except the mono-phosphine-substituted complex **6**, broad singlets were observed at or above room temperature, due to dynamic processes. By VT ^{31}P NMR spectroscopy (representative VT ^{31}P{^{1}H} NMR spectra of compounds **1**−**5** are given as Supporting Information) we were able to observe the restricted pseudorotation of the ligands in complexes **1**−**5** (as depicted in Figures 5 and 6). Due to the broadness of the signals, generally only $^1J_{P,H}$ coupling constants could be detected at room temperature, while in the spectra of the tungsten complexes the $^1J(^{31}P-^{183}W)$ coupling constants, if measurable at all, could only be seen at very low temperature when the line-broadening effect of the pseudorotation had diminished. For the tris-phosphine-substituted complexes, neither $^1J_{P,H}$ nor $^1J(^{31}P-^{183}W)$ could be determined accurately for any of the ligands. However, it can be assumed that the triplets observed at

(27) Ziegler, T.; Tschinke, V.; Ursenbach, C. *J. Am. Chem. Soc.* **1987**, *109*, 4825−4837.
(28) Dörr, M.; Frenking, G. *Z. Anorg. Allg. Chem.* **2002**, *628*, 843−850.
(29) Jonas, V.; Thiel, W. *J. Chem. Phys.* **1995**, *102*, 8474−8484.
(30) Sommer, R.; Lönnecke, P.; Hey-Hawkins, E. *Dalton Trans.* Manuscript in preparation.

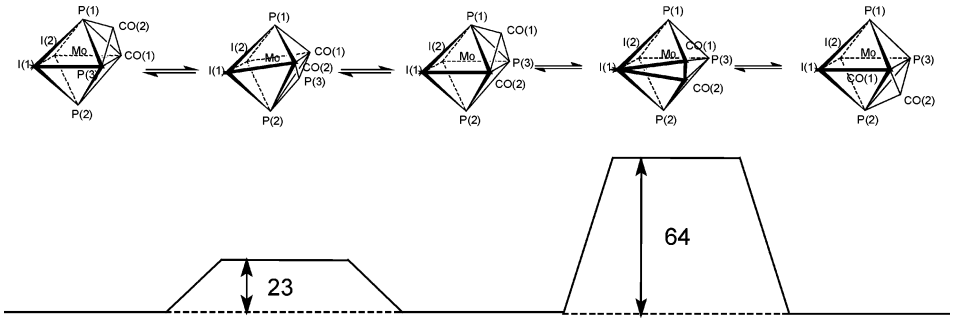

Figure 6. Energy profile for the pseudorotation of the $(CO)_2PH_3$ moiety in the model complex $[MoI_2(CO)_2(PH_3)_3]$ (in kJ/mol).

Table 8. Coalescence Temperature (T_c, in $CDCl_3$) and $^{31}P-^{31}P$, $^{31}P-^{1}H$, and $^{31}P-^{183}W$ Coupling Constants at Low Temperature (T, in $CDCl_3$; for $T = -100$ °C: in THF)

			P_a			P_b			P_n			
complex	T_c,[a] °C	T, °C	δ, ppm	$^1J_{P,H}$, Hz	$^1J_{P,W}$, Hz	δ, ppm	$^1J_{P,H}$, Hz	$^1J_{P,W}$, Hz	δ, ppm	$^1J_{P,H}$, Hz	$^1J_{P,W}$, Hz	$^2J_{P,P}$, Hz, mul.
$[MoI_2(CO)_3(PH_2Fc)_2]$ (**1a**)	−28	−63	−51.1	410		−59.0	388					230 d
$[WI_2(CO)_3(PH_2Fc)_2]$ (**1b**)	−3	−63	−69.9	405	174	−76.0	390	132				205 d
$[MoI_2(CO)_3(PH_2CH_2Fc)_2]$ (**2a**)	−23	−61	−42.4	396		−56.3	369					196 d
$[WI_2(CO)_3(PH_2CH_2Fc)_2]$ (**2b**)	7	−60	−60.0	394	180	−74.5	377	132				182 d
$[MoI_2(CO)_2(PH_2Fc)_3]$ (**3a**)	−13	−63	−36	*b*		−36	*b*		−44.8	*b*		86 t
		−100	−26.5	≈380		−48	*b*		−52	387		
$[WI_2(CO)_2(PH_2Fc)_3]$ (**3b**)	12	−63	−57	*b*	*b*	−57	*b*	*b*	−64.3	393	163	82 t
$[MoI_2(CO)_2(PH_2CH_2Fc)_3]$ (**4a**)	−20	−61	−31	*b*		−31	*b*		−35.3	376		72 t
$[WI_2(CO)_2(PH_2CH_2Fc)_3]$ (**4b**)	−13	−63	−53	*b*	*b*	−53	*b*	*b*	−53.4	*b*	*b*	68 t
		−100	−48	*b*	*b*	−61	*b*	*b*	−51.7	385	*b*	68 t
$[MoI_2(CO)_3\{PH(CH_2Fc)_2\}_2]$ (**5a**)	0	−51	17.2	405		1.1	375					176 d
$[WI_2(CO)_3\{PH(CH_2Fc)_2\}_2]$ (**5b**)	30	−60	−0.6	415	*b*	−19.6	387	*b*				174 d

[a] T_c was determined to be ±5 to 10 K. [b] Broad signals, high noise level, or otherwise poor signal quality.

low temperature in the spectra of complexes **3** and **4** are due to the respective phosphine ligand that is *cis* to the other two phosphine ligands (P3 in Figure 1), on the basis of the relatively small $^2J_{P,P}$ coupling constant in the range between 68 and 86 Hz (see Table 8). A full line-shape analysis was not performed, as in most cases the chemical shift and values of the coupling constant could not be determined unambiguously at low temperatures.

As we were unable to carry out a full line-shape analysis, we tried to model the energy profile of the ligand pseudorotation. For the bis-phosphine model complexes $[MI_2(CO)_3(PH_3)_2]$ (M = Mo, W), the results are shown in Figure 5. A structure with one carbonyl group in a unique equatorial position and the other two CO ligands situated symmetrically above and below the equatorial plane (C_s symmetry) was optimized. This structure turned out to be a first-order saddle point. The imaginary frequency corresponds to pseudorotation of the $(CO)_3$ moiety, which would result in the minimum structure. The calculations indicate a higher energy barrier for tungsten.

The calculated energy profile of ligand pseudorotation in the tris-phosphine complex $[MoI_2(CO)_2(PH_3)_3]$ is displayed in Figure 6. Two structures representing first-order saddle points on the rotation pathway could be localized, both with C_s symmetry. The structure with the third phosphine ligand placed in the capping position is about 23 kJ/mol higher in energy than the minimum structure. When the third phosphine occupies a unique equatorial position and the two carbonyl groups lie symmetrically above and below the equatorial plane, the resulting energy is even 64 kJ/mol higher. In both cases, the imaginary frequency corresponds to rotation of the $PH_3(CO)_2$ moiety.

Bis-phosphine-substituted seven-coordinate complexes allow the observation of one pseudorotational mechanism that is based on the change of the position of the capping carbonyl ligand (see Figure 5). Consequently, the two phosphine ligands change their positions, being either in close vicinity of the capping carbonyl group or *trans* to it.

In contrast, tris-phosphine-substituted complexes show two activation barriers with remarkably different heights (see Figure 6). The process on the right-hand side of Figure 6 transforms the two enantiomers of the complex into one another, but since the capping CO is facing up (signifying the neighborhood of atom P1) at the beginning and facing down (toward atom P2) at the end of the process, it results in an equilibration of the signals of the two ligands *trans* to each other, whereas the signal of the phosphine ligand that takes part in the pseudorotation does not broaden. This process corresponds to the lower of the two pseudorotational energy barriers that could be observed in the ^{31}P NMR spectra. Thus, the signals sharpen at lower temperatures even though the mechanism depicted in Figure 6 (left-hand side) remains active (very low energies were calculated to correspond to the onset of signal broadening below −160 °C).[31]

The coalescence temperatures for compounds **3** and **4** are difficult to determine, because the second re-

(31) Faller, J. W. Stereochemical Nonrigidity: Organometallic Compounds. In *Encyclopedia of Inorganic Chemistry*; King R. B., Ed.; John Wiley and Sons: New York, 1994; pp 3914−3933.

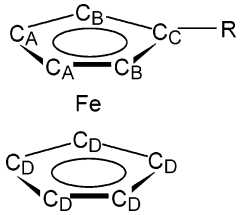

Figure 7. Atom labeling used in NMR assignments of the cyclopentadienyl rings.

arrangement process depicted in Figure 6 (left-hand side) is still active and remains so at temperatures well below −60 °C, while the first ligand-mobility process is "freezing out" (Figure 6, right-hand side). Although this pseudorotational process also has the effect of transforming one enantiomer into the other, this process is not observed in the ^{31}P NMR spectrum, because the neighborhood of either of the axial P atoms remains unchanged, and the transition state is too short-lived to result in an observable signal. We assume this process to take place in solution at temperatures well below −100 °C, as three separate signals with identical intensities could be observed in the $^{31}P\{^1H\}$ NMR spectrum of **3a** and **4b** at −100 °C in THF, which correspond to the three different phosphine ligands in their fixed positions.

Due to the obvious similarities in the spectra of all bis- and all tris-phosphine-substituted complexes, we assume that these two classes of complexes have basically the same structure in solution at low temperature and in the solid state. Thus, in all complexes two (P_a, P_b) or three nonequivalent phosphine ligands (P_a, P_b, P_n) are present (Table 8). The X-ray structure analyses of $[WI_2(CO)_3(PH_2CH_2Fc)_2]$ (**2b**)[3] and $[MoI_2(CO)_2(PH_2CH_2Fc)_3]$ (**4a**) exemplify the structural motif of each class of complexes.

3. Experimental Section

3.1. General Procedures. All reactions were carried out under nitrogen using standard Schlenk line techniques. Solvents were dried and distilled under an inert gas atmosphere prior to application. The primary ferrocenylphosphines PH_2Fc[13] and PH_2CH_2Fc[11] were prepared according to the literature procedures and purified by sublimation. The complexes $[MI_2(CO)_3(NCMe)_2]$ (M = Mo, W)[12] were recrystallized from CH_2Cl_2. $PH(CH_2Fc)_2$ [14] and $[WI_2(CO)_3(PH_2CH_2Fc)_2]$ (**2b**)[3] were prepared according to the literature. NMR spectra were recorded in $CDCl_3$ at 25 °C (if not stated otherwise) using an Avance DRX 400 spectrometer (Bruker). The low-temperature NMR data of **1**−**5** are given in Table 8. NMR tubes were filled under nitrogen and sealed under vacuum. ^1H NMR (400.13 MHz) and ^{13}C NMR (100.3 MHz): external standard TMS, internal standard $CDCl_3$. ^{31}P NMR (161.97 MHz): external standard 85% H_3PO_4 (data are given in Tables 7 and 8). The signals of the C and H atoms in the C_5H_4 groups of the ferrocenyl moiety are labeled according to Figure 7. IR spectra (4000−400 cm^{-1}, KBr disks) were recorded on a Perkin-Elmer Spectrum 2000 FTIR spectrometer (Supporting Information). Selected IR frequencies are given in Table 4. Mass spectra were measured with a Varian MAT 711 (FAB, 70 eV, source temperature 180 °C, matrix 3-NBA). Elemental analysis was performed on a VARIO EL (Heraeus) with handling of the samples in air. The melting points were determined in sealed capillaries under nitrogen and are uncorrected.

3.2. General Procedure for the Synthesis of $[MoI_2(CO)_3L_2]$ (L = PH_2Fc (1a), PH_2CH_2Fc (2a)). A solution of $[MoI_2(CO)_3(NCMe)_2]$ (0.26 g, 0.485 mmol) in CH_2Cl_2 (50 mL) was cooled to −50 °C, and a solution of the corresponding primary ferrocenylphosphine (0.70 mmol) in CH_2Cl_2 (10 mL) that was cooled to ca. −100 °C was added rapidly with stirring. The temperature of the cooling bath was maintained at around −30 °C. After 3 h the solution was concentrated to about 5 mL while keeping it at −30 °C; then pentane (cooled to −100 °C) was added to yield a microcrystalline solid, which was filtered off, washed with pentane (10 mL), and vacuum-dried for 2 h. Yield: 0.30 g of a brown powdery product, which apart from the desired **1a** or **2a** contains **3a** (15%) or **4a** (30%), respectively. Attempts to separate the di- and trisubstituted products by fractional crystallization failed.

1a. Mp: ca. 140 °C (dec). ^1H NMR: δ 4.30 (s, 10 H, H_D), 4.48 and 4.61 (each s, each 4 H, $H_{A,B}$), 6.95 ppm (d, 4 H, $^1J_{P,H}$ = 398 Hz, PH_2). $^{13}C\{^1H\}$ NMR: δ 70.7 (s, C_D), 73.4 and 72.0 ppm (each s, $C_{A,B}$), C_C and CO signals not observed. (Note: only NMR signals of **1a** are listed. Signals of impurity **3a** that appear with ca. 15% intensity are omitted.) MS: *m/z* 871.5 $[M]^+$ (1.0), 843.5 $[MoI_2(CO)_2(PH_2Fc)_2]^+$ (1.0), 658.5 $[MoI(PH_2Fc)_2]^+$ (1.0), 652.5 $[MoI_2(CO)_3(PH_2Fc)]^+$ (0.9), 218.1 $[PH_2Fc]^+$ (100%).

2a. Mp: ca. 187 °C (dec). ^1H NMR: δ 3.31 (br s, 4 H, CH_2), 4.16 (br s, 18 H, $H_{A,B,D}$), 5.61 ppm (d of t, $^1J_{P,H}$ = 378 Hz, $^2J_{P,H}$ = 6.7 Hz, 4 H, PH_2). $^{13}C\{^1H\}$ NMR: δ 24.3 (d, $^1J_{C,P}$ = 12 Hz, CH_2), 68.8 and 69.2 (each s, $C_{A,B}$), 69.7 (s, C_D), 84.9 ppm (s, C_C), CO signals not observed. (Note: only NMR signals of **2a** are listed. Signals of impurity **4a** that appear with ca. 30% intensity are omitted.) MS: *m/z* 976.7 $[MoI(CO)_2(PH_2CH_2Fc)_3]^+$ (from **4a**) (0.3), 899.5 $[M]^+$ (0.4), 871.6 $[MoI_2(CO)_2(PH_2CH_2Fc)_2]^+$ (0.5), 583.7 $[MoI_2(PH_2CH_2Fc)]^+$ (0.3), 515.8 $[MoI(CO)_2(PH_2CH_2Fc)]^+$ (0.4), 232.0 $[PH_2CH_2Fc]^+$ (27.0%).

3.3. General Procedure for the Synthesis of $[WI_2(CO)_3L_2]$ (L = PH_2Fc (1b), PH_2CH_2Fc (2b)). Primary ferrocenylphosphine (0.96 mmol) was added to a solution of $[WI_2(CO)_3(NCMe)_2]$ (0.29 g, 0.48 mmol) in CH_2Cl_2 (20 mL). After stirring for 2 h at rt the solution was filtered over degassed Celite. The solvent was removed from the reaction mixture in vacuo, and the crude product was washed twice with pentane (10 mL) and dried for 1 h. Yield: 0.42 g (91%) of **1b** as a yellow microcrystalline solid or 0.45 g (90%) of **2b**·0.5 CH_3CN·0.5CH_2Cl_2 as a greenish-brown microcrystalline solid. The latter can be recrystallized from THF to give orange single crystals of $[WI_2(CO)_3(PH_2CH_2Fc)_2]$·0.5THF suitable for X-ray crystal structure analysis. Mp, NMR data (^1H, ^{13}C, ^{31}P), and IR data were previously reported.[3] The MS data are given here.

1b. Mp: ca. 145 °C (dec). Anal. Found: C, 28.44; H, 2.46; N, 0.0 (Calcd: C, 28.85; H, 2.32; N, 0.0). ^1H NMR: δ 4.27 (s, 10 H, H_D), 4.47 and 4.59 (each s, each 4 H, $H_{A,B}$), 7.14 ppm (d, $^1J_{P,H}$ = 402 Hz, 4 H, PH_2). $^{13}C\{^1H\}$ NMR: δ 70.9 (s, C_C), 71.0 (s, C_D), 73.3 and 73.7 (2 br s, $C_{A,B}$), 247.1 ppm (s, CO). MS: *m/z* 957.7 $[M]^+$ (3.5), 929.8 $[WI_2(CO)_2(PH_2Fc)_2]^+$ (2.4), 218.1 $[PH_2Fc]^+$ (92.5%).

2b·0.5THF. MS: *m/z* 985.8 $[M]^+$ (3.5), 957.7 $[WI_2(CO)_2(PH_2CH_2Fc)_2]^+$ (2.0), 858.8 $[WI(CO)_3(PH_2CH_2Fc)_2]^+$ (1.5), 830.7 $[WI(CO)_2(PH_2CH_2Fc)_2]^+$ (0.9), 753.6 $[WI_2(CO)_3(PH_2CH_2Fc)]^+$ (1.2), 628.5 $[WI(CO)_3(PH_2CH_2Fc)]^+$ (1.2), 232.1 $[PH_2CH_2Fc]^+$ (100%).

3.4. $[MoI_2(CO)_2(PH_2Fc)_3]$ (3a). $[MoI_2(CO)_3(NCMe)_2]$ (0.12 g, 0.23 mmol) and PH_2Fc (0.16 g, 0.73 mmol) were dissolved in THF (8 mL) with stirring, and the solution was kept at rt for 6 h while orange crystals formed. The solution was decanted off, and the orange crystals were dried in vacuo. The solvent was removed to yield a microcrystalline yellow-orange solid, which was washed with pentane (5 mL) to remove excess PH_2Fc and dried in a vacuum for 2 h. The combined yield was 0.21 g (86%).

Mp: 181 °C (140 °C dec). Anal. Found: C, 35.8; H, 3.21; O, 3.93 (Calcd for **3a**·0.6H_2O: C, 35.90; H, 3.22; O, 3.89). ^1H NMR: δ 4.19 (s, 15 H, H_D), 4.32 and 4.40 (2 s, each 6 H, $H_{A,B}$), 6.48 ppm (d, $^1J_{P,H}$ = 383 Hz, 6 H, PH_2). $^{13}C\{^1H\}$ NMR: δ 70.4 (s, C_C), 70.9 (s, C_D), 71.7 and 74.0 (2 br s, $C_{A,B}$), 238.3 ppm (CO, s). MS (FAB): *m/z* 1061.7 $[M]^+$ (0.7), 1003.8 $[MoI_2(PH_2$-

$Fc)_3]^+$ (0.5), 908.7 $[MoI(CO)(PH_2Fc)_3]^+$ (0.6%), 786.6 $[MoI_2(PH_2Fc)_2]^+$ (1.6), 531.3 $[Mo(PH_2Fc)_2]^+$ (100), 218.1 $[PH_2Fc]^+$ (39%).

3.5. $[WI_2(CO)_2(PH_2Fc)_3]$ (3b). $[WI_2(CO)_3(NCMe)_2]$ (0.37 g, 0.61 mmol) and PH_2Fc (0.40 g, 1.83 mmol) were dissolved in THF (20 mL) and stirred for 24 h. The solvent was removed, and the remaining yellow powder was washed with pentane (10 mL) and dried in a vacuum to yield 0.64 g (91%) of **3b** as a yellow crystalline powder.

Mp: 184 °C (dec, sublimation of PH_2Fc). Anal. Found: C, 33.6; H, 2.04; O, 2.82 (Calcd: C, 33.49; H, 2.89; O, 2.79). ^{1}H NMR: δ 4.19 (s, 15 H, H_D), 4.33 and 4.40 (each s, each 6 H, $H_{A,B}$), 6.76 ppm (br d, $^1J_{P,H}$ = 385 Hz, 6 H, PH_2). $^{13}C\{^1H\}$ NMR: δ ca. 66 (v br, C_C), 70.8 (s, C_D), 71.7 (d, $^3J_{P,C}$ = 6.2 Hz, C_A), 74.0 (d, $^2J_{P,C}$ = 9.5 Hz, C_B), 230.2 and 230.4 ppm (2 s, CO). MS: *m/z* 1147.4 $[M]^+$ (0.7), 1119.3 $[WI_2(CO)(PH_2Fc)_3]^+$ (1.0), 218.1 $[PH_2Fc]^+$ (22%).

3.6. $[MoI_2(CO)_2(PH_2CH_2Fc)_3]$ (4a). $[MoI_2(CO)_3(NCMe)_2]$ (0.11 g, 0.21 mmol) and PH_2CH_2Fc (0.15 g, 0.64 mmol) were dissolved in THF (8 mL). The solution was stirred for 6 h, and the solvent was removed to yield a microcrystalline yellow-orange solid, which was washed with pentane (10 mL) to remove excess PH_2CH_2Fc and dried in a vacuum to give 0.21 g (91%) of an orange powder. Orange rhombohedral crystals suitable for X-ray crystal structure analysis were obtained by recrystallization from $CHCl_3$ at −30 °C.

Mp: 159 °C (155 °C dec). Anal. Found: C, 38.2; H, 3.61; O, 3.00 (Calcd: C, 38.15; H, 3.57; O, 2.90). ^{1}H NMR: δ 3.13 (t of d, $^3J_{H,H}$ = 6.4 Hz, $^2J_{P,H}$ = 4.4 Hz, 6 H, CH_2), 4.16, 4.17 and 4.19 (3 br s, 27 H, $H_{A,B,D}$), 5.21 ppm (d, $^1J_{P,H}$ = 366 Hz, 6 H, PH_2). $^{13}C\{^1H\}$ NMR: δ 24.5 (d, $^1J_{C,P}$ = 25.4 Hz, CH_2), 68.9 and 69.0 (2 s, $C_{A,B}$), 69.7 (s, C_D), 85.2 (s, C_C), 238.3 ppm (s, CO). MS: *m/z* 868.6 $[MoI_2(CO)_2(PH_2CH_2Fc)_2]^+$ (0.5), 616.5 $[Mo(CO)_2(PH_2CH_2Fc)_2]^+$ (3.2), 232.1 $[PH_2CH_2Fc]^+$ (27%).

3.7. $[WI_2(CO)_2(PH_2CH_2Fc)_3]$ (4b). $[WI_2(CO)_3(NCMe)_2]$ (0.36 g, 0.60 mmol) and PH_2CH_2Fc (0.21 g, 1.79 mmol) were dissolved in THF (20 mL) and stirred for 24 h. The solution was filtered over degassed Celite and reduced to half its volume. Pentane (10 mL) was added, and the solution was cooled to −30 °C for 24 h. The solvent was decanted off, and the remaining orange microcrystalline solid was dried in a vacuum. Yield: 0.58 g (78%) of **4b**·0.75THF.

Mp: 78−79 °C (185 °C, dec). Anal. Found: C, 35.6; H, 3.44; O, 3.53 (Calcd for **4b**·0.75THF: C, 36.69; H, 3.64; O, 3.53). ^{1}H NMR: δ 1.85 and 3.75 (each m, each 3 H, THF), 3.17 (br, 6 H, CH_2), 4.08, 4.13 and 4.17 (br, 27 H, $H_{A,B,D}$), 5.49 ppm (br d, $^1J_{P,H}$ = 373 Hz, 6 H, PH_2). $^{13}C\{^1H\}$ NMR: δ 24.4 (br d, CH_2), 26.3 and 68.7 (THF), 69.0 and 69.4 (2 s, $C_{A,B}$), 69.7 (s, C_D), 85.2 ppm (s, C_C), CO signals not observed. MS: *m/z* 1189.8 $[M]^+$ (1.0), 1062.8 $[WI(CO)_2(PH_2CH_2Fc)_3]^+$ (7.0), 955.6 $[WI_2(CO)_2(PH_2CH_2Fc)_2]^+$ (1.3), 831.7 $[WI(CO)_2(PH_2CH_2Fc)_2]^+$ (0.9), 801.8 $[WI(CO)(PH_2CH_2Fc)_2]^+$ (3.0), 772.8 $[WI(PH_2CH_2Fc)_2]^+$ (2.7), 232.1 $[PH_2CH_2Fc]^+$ (100%).

3.8. $[MoI_2(CO)_3\{PH(CH_2Fc)_2\}_2]$ (5a). $[MoI_2(CO)_3(NCMe)_2]$ (0.10 g, 0.20 mmol) and $PH(CH_2Fc)_2$ (0.17 g, 0.40 mmol) were dissolved in CH_2Cl_2 (15 mL). The solution was stirred overnight at rt. After filtration over degassed Celite the solvent was removed in a vacuum. The remaining solid was washed with pentane (10 mL). The product was dried in a vacuum to yield 0.23 g (89%) of a beige solid.

Mp: 187 °C (dec). Anal. Found: C, 43.8; H, 3.48; P, 4.77 (Calcd: C, 43.63; H, 3.58; P, 4.79). ^{1}H NMR: δ 3.14 and 3.38 (2 m, 8 H, CH_2), 4.14 (s, 20 H, H_D), 4.19 and 4.22 (2 s, 16 H, $H_{A,B}$), 5.54 ppm (d, $^1J_{P,H}$ = 389 Hz, 2 H, PH). $^{13}C\{^1H\}$ NMR: δ 23.2 (d, $^1J_{C,P}$ = 31.7 Hz, CH_2), 69.3 and 70.0 (2 s, $C_{A,B}$), 69.7 (s, C_D), 82.9 ppm (s, C_C), CO signals not observed. MS: *m/z* 1293.7 $[M]^+$ (1.7), 1265.6 $[MoI_2(CO)_2\{PH(CH_2Fc)_2\}_2]^+$ (2.2), 1209.8 $[MoI_2\{PH(CH_2Fc)_2\}_2]^+$ (4.9), 1141.1 $[MoI(CO)_2\{PH(CH_2Fc)_2\}_2]^+$ (3.7), 1083.2 $[MoI\{PH(CH_2Fc)_2\}_2]^+$ (7.6), 780.4 $[MoI_2\{PH(CH_2Fc)_2\}]^+$ (6), 654.0 $[MoI\{PH(CH_2Fc)_2\}]^+$ (8), 430.2 $[PH(CH_2Fc)_2]^+$ (100), 231.2 $[PHCH_2Fc]^+$ (99%).

3.9. $[WI_2(CO)_3\{PH(CH_2Fc)_2\}_2]$ (5b). $[WI_2(CO)_3(NCMe)_2]$ (0.12 g, 0.20 mmol) and $PH(CH_2Fc)_2$ (0.17 g, 0.40 mmol) were dissolved in THF (15 mL). The solution was stirred overnight at room temperature. After filtration over degassed Celite the solvent was removed in a vacuum. The remaining solid was washed with pentane (10 mL). The product was dried in a vacuum to yield 0.24 g (84%) of an orange microcrystalline solid.

Mp: 149 °C (dec). Anal. Found: C, 40.7; H, 3.24; O, 3.21; P, 4.48 (Calcd: C, 40.85; H, 3.36; O, 3.44; P, 4.17). ^{1}H NMR: δ 3.19 and 3.43 (2 m, 8 H each, CH_2), 4.13 (s, 20 H, H_D), 4.17 and 4.21 (2 s, 16 H, $H_{A,B}$), ca. 5.8 ppm (v. br d, $^1J_{P,H}$ ca. 400 Hz, 2 H, PH). $^{13}C\{^1H\}$ NMR: δ 26.2 (d, $^1J_{C,P}$ = 21.4 Hz, CH_2), 68.9, 69.3, 69.6, and 70.1 (4 s, $C_{A,B}$), 69.7 (s, C_D), 82.9 ppm (s, C_C), CO signals not observed. ^{31}P NMR (+40 °C): δ ca. −15 ppm (v br); see Tables 7 and 8. MS: *m/z* 1381.5 $[M]^+$ (3.7), 1353.4 $[WI_2(CO)_2\{PH(CH_2Fc)_2\}_2]^+$ (0.5), 1254.5 $[WI(CO)_3\{PH(CH_2Fc)_2\}_2]^+$ (1.0), 1226.5 $[WI(CO)_2\{PH(CH_2Fc)_2\}_2]^+$ (1.1), 1198.4 $[WI(CO)\{PH(CH_2Fc)_2\}_2]^+$ (0.3), 1183.4 $[WI_2(CO)_3\{PH(CH_2Fc)_2\}(PHCH_2Fc)]^+$ (1.1), 1168.5 $[WI\{PH(CH_2Fc)_2\}_2]^+$ (0.6), 951.6 $[WI_2(CO)_3\{PH(CH_2Fc)_2\}]^+$ (65), 922.5 $[WI_2(CO)_2\{PH(CH_2Fc)_2\}]^+$ (0.5), 738.7 $[WI\{PH(CH_2Fc)_2\}]^+$ (1.4), 729.0 $[W(CO)_2(PHCH_2Fc)_2]^+$ (2.0), 613.0 $[W\{PH(CH_2Fc)_2\}]^+$ (3.1), 429.9 $[PH(CH_2Fc)_2]^+$ (100), 231.0 $[PHCH_2Fc]^+$ (71%).

3.10. $[WI_2(CO)_3(NCMe)\{PH(CH_2Fc)_2\}]$ (6). $PH(CH_2Fc)_2$ (0.09 g, 0.21 mmol) was added to a solution of $[WI_2(CO)_3(NCMe)_2]$ (0.13 g, 0.22 mmol) in CH_2Cl_2 (10 mL) with stirring. After 30 min the solution was filtered over degassed Celite, and the solvent was removed in a vacuum. The remaining solid was washed with pentane (5 mL). The product was dried in a vacuum to yield 0.20 g (96%) of an orange solid, which can be recrystallized from CH_2Cl_2 (5 mL) at −20 °C to give single crystals of $[WI_2(CO)_3(NCMe)\{PH(CH_2Fc)_2\}]$ suitable for X-ray crystal structure analysis.

Mp: ca. 100 °C (dec). Anal. Found: C, 32.4; H, 2.78; N, 1.54; O, 5.01 (Calcd: C, 32.66; H, 2.64; N, 1.41; O 4.83). ^{1}H NMR: δ 2.19 (br s, 3 H, CH_3CN), 3.19 (br s, 4 H, CH_2), 4.14, 4.17, and 4.22 (each s, 18 H, $H_{A,B,D}$), 5.04 ppm (br d, $^1J_{P,H}$ = 388 Hz, 1 H, PH). $^{13}C\{^1H\}$ NMR: δ 26.3 (d, $^1J_{C,P}$ = ca. 25 Hz, CH_2), 27.9 (br s, CH_3), 69.0, 69.3, 69.8, 70.0, 70.1, and 70.4 (s, $C_{A,B,D}$), 82.2 and 83.0 ppm (s, C_C), CN and CO signals not observed. ^{31}P NMR: see Table 7. $^{31}P\{^1H\}$ NMR: δ 7.6 ppm (d, $^1J_{P,W}$ = 163 Hz). MS: *m/z* 951.8 $[WI_2(CO)_3\{PH(CH_2Fc)_2\}]^+$ (2.5), 923.8 $[WI_2(CO)_2\{PH(CH_2Fc)_2\}]^+$ (1.3), 865.9 $[WI(CO)_3(NCMe)\{PH(CH_2Fc)_2\}]^+$ (0.9%), 738.9 $[W(CO)_3(NCMe)\{PH(CH_2Fc)_2\}]^+$ (1.1%), 642.8 $[W(CO)\{PH(CH_2Fc)_2\}]^+$ (1.3), 612.2 $[W\{PH(CH_2Fc)_2\}]^+$ (4.1), 560.1 $[WI_2(CO)_3(NCMe)]^+$ (3.4), 430.1 $[PH(CH_2Fc)_2]^+$ (84), 231.0 $[PHCH_2Fc]^+$ (67), 200.1 $[FcCH_3]^+$ (100%).

3.11. Density Functional Theory (DFT) Calculations. Density functional theory (DFT) calculations with the widely used B3LYP functionals[32,33] were performed using the Gaussian98 program package.[34] For the metal atoms and for iodine, relativistic effective core potentials replacing the 10 and 50 inner core electrons, respectively, and the corresponding valence basis sets were used.[35] The standard 6-31G* basis set was applied for the other atoms.[36]

(32) Becke, A. D. *J. Chem. Phys.* **1993**, *98*, 5648−5652.
(33) Lee, C.; Yang, W.; Parr, R. G. *Phys. Rev. B* **1988**, *37*, 785−789.
(34) Frisch, M. J.; Trucks, G. W.; Schlegel, H. B.; Scuseria, G. E.; Robb, M. A.; Cheeseman, J. R.; Zakrzewski, V. G.; Montgomery, J. A., Jr.; Stratmann, R. E.; Burant, J. C.; Dapprich, S.; Millam, J. M.; Daniels, A. D.; Kudin, K. N.; Strain, M. C.; Farkas, O.; Tomasi, J.; Barone, V.; Cossi, M.; Cammi, R.; Mennucci, B.; Pomelli, C.; Adamo, C.; Clifford, S.; Ochterski, J.; Petersson, G. A.; Ayala, P. Y.; Cui, Q.; Morokuma, K.; Malick, D. K.; Rabuck, A. D.; Raghavachari, K.; Foresman, J. B.; Cioslowski, J.; Ortiz, J. V.; Stefanov, B. B.; Liu, G.; Liashenko, A.; Piskorz, P.; Komaromi, I.; Gomperts, R.; Martin, R. L.; Fox, D. J.; Keith, T.; Al-Laham, M. A.; Peng, C. Y.; Nanayakkara, A.; Gonzalez, C.; Challacombe, M.; Gill, P. M. W.; Johnson, B. G.; Chen, W.; Wong, M. W.; Andres, J. L.; Head-Gordon, M.; Replogle, E. S.; Pople, J. A. *Gaussian 98*, revision A.9; Gaussian, Inc.: Pittsburgh, PA, 1998.
(35) Hay, P. J.; Wadt, W. R. J. *J. Chem. Phys.* **1985**, *82*, 299−310.

3.12. X-ray Analysis. Data were collected with a Siemens CCD (SMART) diffractometer (ω-scans). Data reduction was performed with SAINT, including SADABS, a program for empirical absorption correction. The structure was solved by direct methods, and non-hydrogen atoms were refined anisotropically (SHELX97). All H atoms were calculated on idealized positions. Pictures were generated with ORTEP for Windows.[23,24,37]

Crystallographic data can be obtained free of charge via www.ccdc.cam.ac.uk/conts/retrieving.html (or from the Cambridge Crystallographic Data Centre, 12 Union Road, Cambridge CB2 1EZ, UK; fax: (+44) 1223-336-033; or deposit@ccdc.cam.uk). Any request to the CCDC for material should quote the full literature citation and the references CCDC 166297 (**2b**), 223147 (**4a**), and 223146 (**6**).

Acknowledgment. Financial support from INTAS (00-00677) and the Deutscher Akademischer Austauschdienst (DAAD/ARC 313-ARC-XIII-99/40, R.S., DAAD 313, A/01/45669, P.K.B.) is gratefully acknowledged.

Supporting Information Available: IR data, VT NMR spectra of **1b**, **2b**, **3b**,**4a**, **4b**, and **5a**, and catalytic properties of **1**−**4** are available free of charge via the Internet at http://pubs.acs.org.

OM0501982

(36) Hehre, W. J.; Radom, L.; Schleyer, P. v. R.; Pople, J. A. *Ab initio Molecular Orbital Theory*; Wiley: New York, 1986.

(37) (a) *SMART*: Area-Detector Software Package; Siemens Industrial Automation, Inc.: Madison, WI, 1993. (b) *SAINT*: Area-Detector Integration Software, Version 6.01; Siemens Industrial Automation, Inc.: Madison, WI, 1999. (c) Sheldrick, G. M. *SADABS*: Program for Scaling and Correction of Area-detector Data; Göttingen, 1997. (d) *ORTEP3 for Windows*: Farrugia, L. J. *J. Appl. Crystallogr.* **1997**, *30*, 565.